Journal of
Applied Crystallography
ISSN 0021-8898

Received 16 August 2006
Accepted 5 January 2007

Density fluctuations in oxide glasses investigated by small-angle X-ray scattering

Claire Levelut,[a]* Rozenn Le Parc,[a] Annelise Faivre,[a] Ralf Brüning,[c] Bernard Champagnon,[b] Valérie Martinez,[b] Jean-Paul Simon,[d] Françoise Bley[d] and Jean-Louis Hazemann[e]

[a]Laboratoire des Colloides, Verres et Nanomatériaux, CNRS UMR 5587, Université Montpellier II, 34095 Montpellier Cedex, France, [b] Université de Lyon, Lyon, F-69003, France; Université Lyon 1, Villeurbanne, F-69622, France; CNRS, UMR5620, Laboratoire de Physico-Chimie des Matériaux Luminescents, Villeurbanne, F-69622, France, [c]Physics Department, University Mount Allison, Canada, [d]Laboratoire de Thermodynamique et Physicochimie Métallurgiques, UMR 5614, INP et UJF Grenoble, BP 75, 38402 Saint Martin d'Hères, France, and [e]Laboratoire de Cristallographie, UPR 5031, 26 avenue des Martyrs, BP 166, 38042 Grenoble Cedex 9, France. Correspondence e-mail: claire@lcvn.univ-montp2.fr

The structure of glasses is characterized by the existence of density and composition fluctuations on the nanometre scale. We present three examples of the use of small-angle X-ray scattering to get information about these density fluctuations. The thermal history and OH content were observed to have a huge influence. The static compressibility decreases when the OH content or fictive temperature increase. We showed that temperature scanning small-angle X-ray scattering can provide an accurate description of the position, width and shape of the glass transition.

© 2007 International Union of Crystallography
Printed in Singapore – all rights reserved

1. Introduction

Not much is known about the intermediate-range order in glasses, although an understanding of it is of fundamental interest because it determines many properties, such as mechanical or transport properties. Fluctuations of density and composition in multicomponent glasses are expected to take place on the nanometre scale. These fluctuations, characteristic of disorder, include dynamical fluctuations (for example, vibrational modes or phonons) and static fluctuations, which are frozen in at the glass transition upon cooling down a liquid to form a glass. Silica glass is suitable for a thorough study of density fluctuations because there are no composition fluctuations in this monocomponent glass.

We present three applications of the determination of density fluctuations using small-angle X-ray scattering (SAXS) measurements in silica glasses. We studied the influence of thermal history and hydroxyl content on the amplitude of the density fluctuations; we determined the isothermal compressibility in silica glasses; and we used temperature scanning SAXS to get information about the glass transition (position, shape and width).

2. Samples and experiments

We studied three kinds of silica glasses of different origin. One of them was a high purity silica sample (with very low OH content) of type I (Brückner, 1970). For this silica glass, which will be called silica A in the following, several samples with different well defined thermal histories were prepared by thermal annealing in the glass transition range, as previously described (Levelut *et al.*, 2002; Le Parc *et al.*, 2002). Spectroscopic features sensitive to the thermal history (Agarwal & Tomozawa, 1995; Geissberger & Galeener, 1983) were measured to check that the thermal heat treatment at a fixed temperature had been long enough to ensure the 'stabilization' of the glass structure (Champagnon *et al.*, 2000; Le Parc *et al.*, 2001). It is convenient to characterize simple thermal histories (such as stabilization by thermal annealing in the glass transition range and fast quenching) by the fictive temperature, T_f, introduced by Tool & Eichlin (1931), at which the structure is frozen in. In the present case, the fictive temperature is equal to the annealing temperature. The influence of thermal history on the amplitude of the density fluctuations was studied in these samples as a function of temperature, from room temperature to about 1773 K, by increasing the temperature step by step. The isothermal compressibility was determined in the glass transition range and in the supercooled liquid state.

Scanning temperature SAXS measurements were performed on two samples with different hydroxyl contents: sample B is a sample of GE-124 ([OH] = 2 ± 1 wt. p.p.m.) and sample C is a sample of Corning 7980 ([OH] = 832 ± 6 wt. p.p.m.). The initial thermal history of these samples is not known. Measurements were carried out with heating rates of 10, 40 and 80 K min^{-1}. At least three cooling and heating ramps were measured for each sample.

The small-angle X-ray scattering measurements were performed on the D2AM experimental setup of the European Synchrotron Radiation Facility (ESRF) in Grenoble, France. The measurements were performed on small plates of about 1 mm thickness. At the maximum temperature of measurement, in the supercooled liquid state, the viscosity remains sufficiently high to prevent deformation of the free-standing samples and no special container is needed. The data for the silica samples were measured with an incident energy of 18 keV in a high temperature molybdenum furnace already referred to (Soldo *et al.*, 1998). This setup yields an available q range of 0.02–0.7 Å^{-1}, where $q = (4\pi/\lambda)\sin\theta$ is the modulus of the scattering vector and θ is half of the scattering angle. The data were collected using a charge coupled device (CCD) camera. The accumulation times were 200 s for measurements at fixed temperature, 20 s for scanning rates of 10 and 40 K min^{-1} and 10 s for temperature scanning experiments with scanning rates of 80 K min^{-1}. The temperatures in the furnace were calibrated by observing the melting of a gold

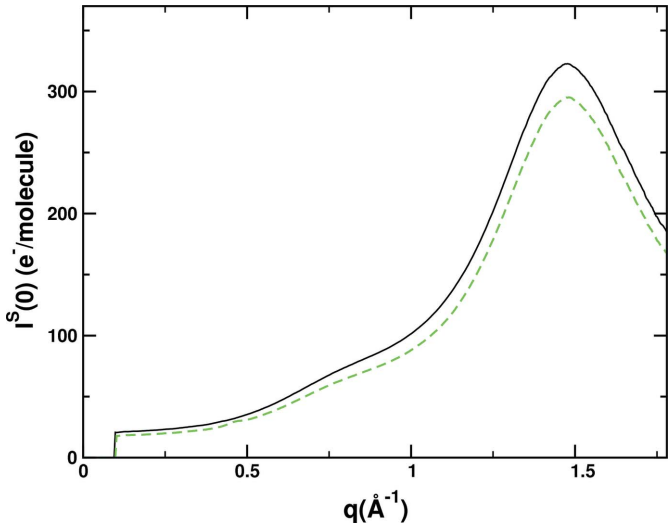

Figure 1
Scattering intensity as a function of modulus of scattering vector in two samples of silica A with different thermal histories: one sample heat-treated at 1523 K (solid line) and one sample heat-treated at 1373 K (dashed line).

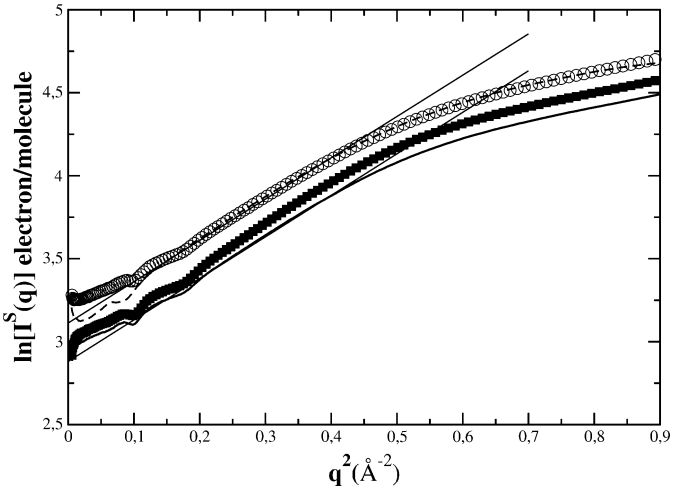

Figure 2
Logarithm of the scattering intensity plotted *versus* q^2 for the three samples at room temperature: silica A annealed at 1533 K, measured at room temperature (open circles), sample B (solid line) and sample C (black squares). Comparison with high-temperature measurements (1773 K) (dashed line). This plot exhibits a linear regime at small q values in which extrapolation using equation (5) can be performed. Two examples of linear fits are shown with thin solid lines.

foil, which deviates less than 2 K from the standard value. Radial integration and corrections for cosmic rays were performed in the usual way. The X-rays were monitored before the furnace, m_0, and after the furnace, m_1, by scattering part of the beam with Kapton foils onto scintillation counters. Before measuring a new sample, the SAXS signal of the empty furnace, $I^{\rm B}(q)$, was systematically measured. This background originated mainly from the Kapton windows and air scattering.

Based on the measured signal with the sample in place, $I^{\rm S+B}(q)$, the signal originating from the sample was calculated according to

$$I^{\rm S}(q) \propto (t \ln 1/t)^{-1}\{[I^{\rm S+B}(q)/m_1^{\rm S+B}] - [I^{\rm B}(q)/m_1^{\rm B}]\}(m_1^{\rm S+B}/m_0^{\rm S+B}), \quad (1)$$

where the transmission factor $t = (m_1^{\rm S+B}m_0^{\rm B})/(m_0^{\rm S+B}m_1^{\rm B})$ allows for changes in the thickness and orientation of the sample. In doing this, the signal is corrected for the variations in the incident flux and is normalized to the absorption of the sample. The absolute intensity of the sample is determined by normalization to a reference sample of pure water 1 cm thick. The scattering power of the water sample is taken as 6.37 electron units per molecule H_2O (Levelut & Guinier, 1967). The error in the final absolute intensity is estimated to be about ±2%.

Examples of scattering curves for two samples of silica A annealed at two different temperatures are shown in Fig. 1. The main characteristics of these scattering curves are the so-called first sharp diffraction peak (FSDP) or 'amorphous halo' around $q = 1.5$ Å^{-1} and the nearly flat signal (very slightly increasing with increasing q, due to the low q tail of the FSDP) at lower q. The low q limit of the amplitude of the signal in this flat region is related to the amplitude of the density fluctuations. It has been shown (Wendorff & Fischer, 1973; Roe & Curro, 1983) that

$$\lim_{q\to 0} I^{\rm S}(q) = \rho_{\rm e} \lim_{v\to\infty} \psi(v), \quad (2)$$

where

$$\psi(v) = \frac{\langle N^2\rangle - \langle N\rangle^2}{\langle N\rangle} \quad (3)$$

is the fluctuation function of the number of electrons, N, in a volume v, $\rho_{\rm e}$ is the electron density, defined by

$$\rho_{\rm e} = \rho_0 \frac{(\sum Z)N_{\rm a}}{m}, \quad (4)$$

where m is the molar mass of the molecule, $N_{\rm a}$ is Avogadro's number, ρ_0 the macroscopic density, and $\sum Z$ is the total number of electrons in the molecule.

To analyse the amplitude of the density fluctuations, we extract the low q limit of the intensity using a linear extrapolation law of the type

$$I^{\rm S}(q) = I^{\rm S}(q=0)\exp(bq^2), \quad (5)$$

as already described (Brüning *et al.*, 2005; Levelut *et al.*, 2005). This extrapolation law comes from the observation that $\log[I^{\rm S}(q)]$, plotted as a function of q^2, shows a linear behaviour over a rather large q range. This procedure allowed us to get rid of the low q signal not inherent to sample in the present case.[1] Fig. 2 shows the linear behaviour for three examples of scattering curves $I^{\rm S}(q)$ for $q^2 = 0.1$ to 0.5 Å^{-2}, corresponding to $q = 0.3$ to 0.7 Å^{-1}. The resulting extrapolated intensities, $I^{\rm S}(q=0)$, are plotted in Fig. 3 as a function of temperature, where the measurements are temperature scanning measurements or step by step. The temperature scanning measurements for samples B and C are shown upon heating.

3. Results and discussion

3.1. Influence of thermal history and OH content on the amplitude of the density fluctuations

The first observation that can be deduced from Fig. 3 is that the hydroxyl content and the thermal history affect the amplitude of the density fluctuations significantly and to similar extents. At room temperature, the difference between a quenched A sample ($T_{\rm f}$ = 1773 K) and a low temperature annealed one ($T_{\rm f}$ = 1373 K) is about 20%, and the difference between sample C ([OH] = 900 p.p.m.) and sample B ([OH] = 2 p.p.m.) is about 15%. Increasing the fictive temperature results in an increase of the amplitude of the density

[1] Precise SAXS measurements devoted to the low q region showed that the SAXS intensity in amorphous silica decreases down to $q = 0.01$ Å^{-1} (Levelut & Guinier, 1967; Renninger & Uhlmann, 1974).

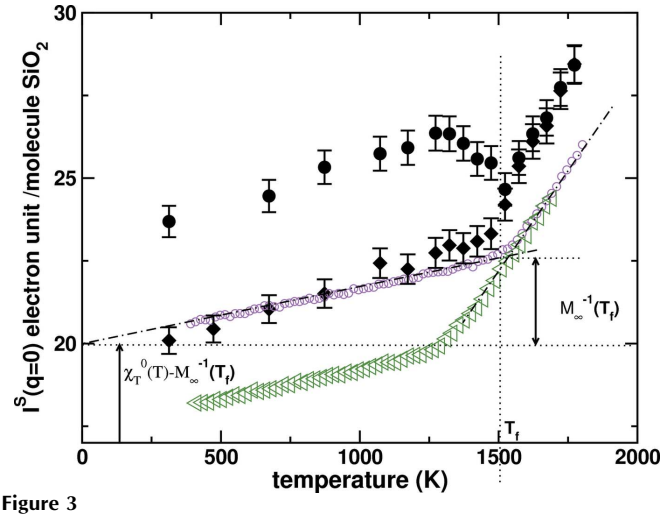

Figure 3
Scattering intensity extrapolated to $q = 0$ using equation (5), plotted as a function of temperature of measurement for different silica samples: sample A ([OH] = a few p.p.b.) annealed at 1373 K (black diamonds) and annealed at 1773 K (black circles), sample B ([OH] = 2 p.p.m., open circles) and sample C ([OH] = 900 p.p.m., open triangles). The dotted-dashed lines indicate how a 'fictive temperature' is determined for samples whose thermal histories are not well defined. The dotted lines show from which intensities $\chi_T^0(T_f) - M_\infty^{-1}(T_f)$ and $M_\infty^{-1}(T_f)$ are determined.

fluctuations. Increasing the OH content decreases the viscosity and thus the glass transition temperature. Although the thermal histories of samples B and C are not known, we could determine the temperature at which the samples are frozen in on the scale probed by SAXS by estimating the intersection of the curves $I^S(q = 0)$ *versus* T for the glass state and for the supercooled liquid, as shown in Fig. 3. An increase of this 'fictive' temperature is then observed between the OH-rich sample C and sample B, which is poor in OH groups. The increase in density fluctuations with decreasing OH content is partly related to the increase in the fictive temperature associated with the decreasing OH content. However, it can also be linked to the increase of the rigidity of the network (LeParc *et al.*, 2006) (increasing the number of bridging oxygens), which prevents the sample from relaxing towards a more homogeneous structure.

On increasing the temperature, one observes a slight increase of the scattering intensity up to the glass transition temperature and then a change of regime at the glass transition temperature, with a steeper slope. The scattering intensities for different samples of silica A with different thermal histories are superimposed in the liquid state. The scattering intensities for samples B and C are also superimposed in the liquid state but on a different curve to silica A. This difference could be ascribed to the presence of Al impurities in silica A.[2] It should also be noted that during the temperature scanning measurements, an evolution of the absolute intensity, by a few per cent, is observed. We rescaled to the measurements taken during the first heating ramp, which were taken as a reference. The evolution could be due to a change in the OH content during the measurements or an evolution of the thermal history. However, the observed change in OH content has been proven to be very weak (Brüning *et al.*, 2005) and the shape of the curve does not change during the successive temperature ramps, as would be expected with a change of thermal history (LeParc *et al.*, 2002; Levelut *et al.*, 2002).

Indeed, the differences observed in the glass transition range, roughly between 1250 and 1600 K, for the two $I^S(q = 0)$ *versus* T curves corresponding to samples of silica A are due to the different thermal histories. The upper curve corresponds to a sample annealed at a temperature (1773 K) located in the upper part of the glass transition interval and then quickly quenched. This sample has a short relaxation time, τ, defined by:

$$\tau = (\eta/G_\infty), \tag{6}$$

where G_∞ is the high-frequency shear modulus, whose variation with temperature is relatively slow (see, for example, LeParc *et al.*, 2006; Polian *et al.*, 2002) and η is the viscosity. Because the latter drastically decreases with decreasing temperature in the glass transition range, τ varies approximately like η. Due to the short τ the sample relaxes during the time of the SAXS measurements and the scattering intensity evolves towards that of a sample that would have been annealed at a lower temperature. The lowest of the two curves for silica A corresponds to the sample annealed at 1373 K, in the lower region of the glass transition interval. This sample has a very long relaxation time and cannot equilibrate during the time of the measurements, and a 'delay' on reaching the supercooled liquid curve is observed upon heating: the sample stays on the glass curve at temperatures higher than would be expected from the intersection of the liquid and solid (glassy) curves for this annealing temperature. At a temperature slightly above this intersection, the relaxation time becomes short enough compared to the measuring time that the scattering intensity joins the supercooled liquid curve.

3.2. Determination of compressibility

The amplitude of the density fluctuations is related to the compressibility of the material. In simple liquids in thermodynamic equilibrium, the extrapolated scattering intensity is simply proportional to the static isothermal compressibility χ_T^0 (Diu *et al.*, 1989):

$$\frac{I^S(q=0)}{N_a\left(\sum Z\right)^2(\rho_0/m)} = k_b T \chi_T^0(T), \tag{7}$$

where k_b is Boltzmann's constant and T is the temperature of the measurements. In a glass, the description has to take into account that part of the fluctuations that are frozen in at the glass transition. Several descriptions have been proposed (Weinberg, 1963; Wendorff & Fischer, 1973; Laberge *et al.*, 1973; Roe & Curro, 1983; Curro & Roe, 1984; Wright *et al.*, 2005). We followed that of Laberge (Laberge *et al.*, 1973), which assumes that the fluctuations not frozen in below the glass transition arise from long-wavelength propagating vibrational modes due to high-frequency longitudinal phonons. Laberge thus introduced the high-frequency longitudinal modulus $M_\infty = \rho_0(V_l^\infty)^2$, where V_l^∞ is the high-frequency longitudinal sound velocity, measured for example using Brillouin light scattering. The extrapolated scattering intensity can then be expressed as a temperature-dependent term proportional to M_∞^{-1} and a frozen-in term, independent of temperature, proportional to the fictive temperature T_f and to the difference between the isothermal compressibility and M_∞^{-1}:

$$\frac{I^S(q=0)}{N_a\left(\sum Z\right)^2(\rho_0/m)} = k_b T_f[\chi_T^0(T_f) - M_\infty^{-1}(T_f)] + k_b T M_\infty^{-1}(T). \tag{8}$$

The isothermal compressibility as a function of temperature T in the glass transition range can be deduced in the supercooled liquid by linear regression, using equation (7). Linear regression also allows the isothermal compressibility at T_f to be determined, using equation (8) and

$$\chi_T^0(T_f) = [\chi_T^0(T_f) - M_\infty^{-1}(T_f)] + M_\infty^{-1}(T_f). \tag{9}$$

[2] Sample A contains around 10 p.p.m. Al_2O_3 whereas samples B and C contain less than 1 p.p.m. Al_2O_3. Changing the Al content is expected to change the compression modulus and the compressibility.

Table 1
Compressibility (10^{-11} m kg^{-1} s^{-2}) determined as indicated in Fig. 3, using the intensity value at T_f divided by the electron density, the Boltzmann constant and the fictive temperature.

The frozen-in and vibrational contributions to the compressibility are determined from the values of the intensity for $T = 0$ K and from the increase in intensity between T_f and 0 K, respectively. For samples B and C, the fictive temperatures are determined from the intersection of $I^S(0)$ *versus* T in the supercooled liquid regime and in the glass regime. This determination of T_f is less accurate than the determination of T_f for samples A of well defined thermal history. The errors bars are 3 or 4% on each value (2% on the intensities and 1% on the fictive temperature for samples A, 2% for samples B and C).

Silica	$\chi_T^0(T_f) - M_\infty^{-1}(T_f)$ frozen in	$M_\infty^{-1}(T_f)$ vibrational	$\chi_T^0(T_f)$ total
Silica A (T_f = 1373 K)	5.08 ± 0.15	0.94 ± 0.03	6.02 ± 0.18
Silica A (T_f = 1773 K)	4.71 ± 0.14	0.94 ± 0.03	5.65 ± 0.17
Silica C (T_f = 1320 K)	4.82 ± 0.20	0.65 ± 0.02	5.47 ± 0.22
Silica B (T_f = 1521 K)	4.79 ± 0.19	0.58 ±0.02	5.37 ± 0.21

Equivalently, the isothermal compressibility in the glass state at T_f can be deduced by dividing $I^S(q=0)/[N_a(\sum Z)^2(\rho_0/m)]$ by k_b and T_f. The extrapolated intensity at $T = 0$ corresponds to the frozen-in part, and the increase between 0 and T_f to the vibrational term, as indicated in Fig. 3. Table 1 presents compressibility data in the glassy state for two samples of silica A, as well as silicas B and C obtained using this method. These analyses assume that the compressibility does not depend on the temperature. Another method is to perform a point by point analysis, as developed in Levelut *et al.* (2005). We determined $\chi_T^0(T)$ in the liquid by dividing each experimental intensity by the temperature. We also determined $\chi_T^0(T_f) - M_\infty^{-1}(T_f)$ in the glass by subtracting $M_\infty^{-1}(T_f) \times T_f$, determined from Brillouin light scattering measurements from the quantity $I^S(q=0)/[N_a(\sum Z)^2(\rho_0/m)]$. Then $\chi_T^0(T_f)$ can be easily deduced. The compressibilities obtained by the different methods are shown in Fig. 4. The determinations in the glassy (open symbols) and in the liquid state (filled symbols) are very close. The compressibility in the glassy state decreases slightly with T_f within experimental uncertainty. The different analysis methods (point by point or assuming that the compressibility is independent of temperature) are in agreement, taking into account the error bars. One important result is the fact that the compressibilities of samples B and C are lower than that of silica A, taking into account the fictive temperature variations. An increase of OH content from a few p.p.b. (silica A) to 2 p.p.m. (sample B) is already sufficient to induce a noticeable decrease of the compressibility. However, it could be noted that another difference between silicas A and B is the existence of Al impurities in silica A, which could also change the compressibility value.

Finally, increasing the fictive temperature or the OH content decreases the compressibility.

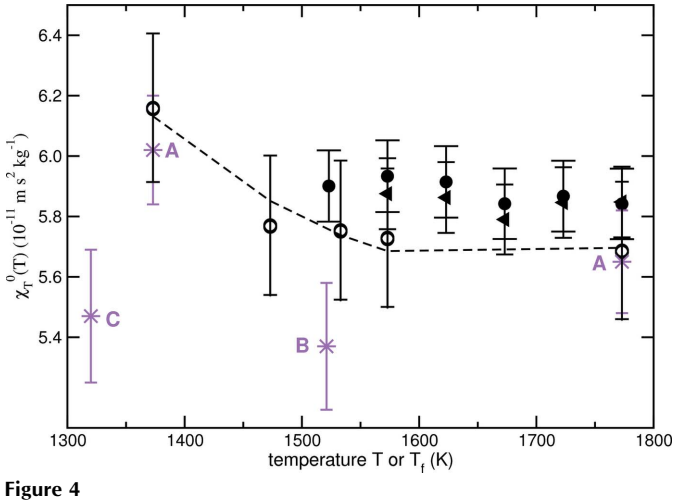

Figure 4
Compressibility determined as shown in Fig. 3, in two samples A with different thermal histories and in silicas B and C (stars). The samples are labelled close to the symbols. Isothermal compressibility in two samples of silica A, annealed at 1373 K (black triangles) and 1773 K (black circles), determined in the liquid state using equation (7) and point by point analysis (Levelut *et al.*, 2005), plotted as a function of temperature. χ_T^0 determined using equation (8) and point by point analysis in the glass state state (open circles) for five samples of silica A plotted as a function of T_f, the temperature of heat treatment (Levelut *et al.*, 2005). The dashed line is a guide for the eye of $\chi_T^0(T_f)$ in the glass state.

3.3. Temperature scanning SAXS

We have seen in §3.1 that the SAXS intensity, extrapolated to $q = 0$ is sensitive to structural relaxation in the glass transition region. $I^S(q=0)$ is different for annealed and quenched samples in the temperature range where scanning calorimetry measurements show differences. Scanning calorimetry is a very commonly used tool for determining the glass transition temperature, T_g, and the relaxation state of glasses, but for vitreous silica, due to the high T_g, such measurements are difficult. We used high-temperature small-angle X-ray scattering (SAXS) experiments as an alternative to calorimetry measurements. Fig. 5(a) shows temperature scanning measurements taken upon heating and upon cooling for silicas B and C. The glass transition region is marked by a hysteresis between the

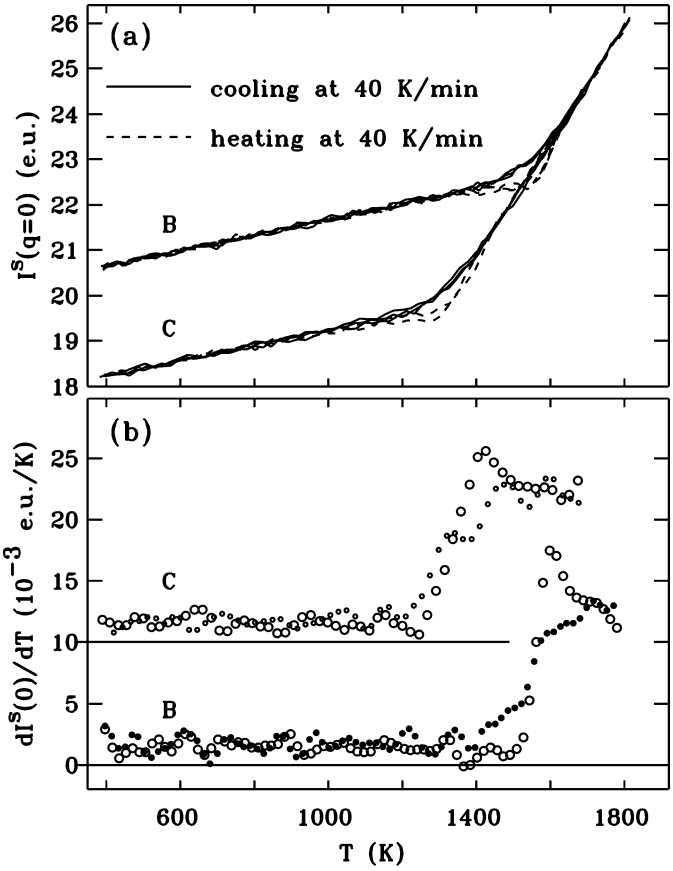

Figure 5
(a) Scattering intensity, measured at 40 K min^{-1} and extrapolated to q = 0, as a function of temperature for samples B and C, measured upon heating (dashed lines) and upon cooling (solid lines). (b) Temperature derivatives of $I^S(0)$ data obtained at 40 K min^{-1} for samples B and C. For clarity, sample C is shifted up by 10×10^{-3} e.u. K^{-1}. T_g is found to be 1535 K for sample B ([OH] = 2 p.p.m.) and 1303 K for sample C ([OH] = 900 p.p.m.).

heating and cooling curves. We considered the temperature derivative of $I^S(q = 0)$, which provides curves that are comparable to calorimetric measurements. High frequencies are enhanced by numeric differentiation; they were partially suppressed by applying a Fourier filter to the differentiated data. The derivative signals obtained for samples B and C are shown in Fig. 5(b). The differentiated curves emphasize the hysteresis of the glass state between heating and cooling. A detailed quantitative analysis (Brüning, 2003; Hodge, 1994) has been performed as described in Brüning *et al.* (2005). This analysis is based on the complete cooling and heating traces. The SAXS data provide tighter constraints on the fit as well as a superior signal-to-noise ratio compared to previous calorimetry data, so that the fit parameters obtained in Brüning *et al.* (2005) are more reliable than the values given previously (Brüning, 2003). The glass transition can be determined from the low-temperature limit of the fictive temperature calculated from the cooling curve of the best fit of the data to the model. The glass transition of silica C, with a higher water content, is 232 ± 14 K lower than the glass transition of silica B (water content 2 p.p.m.). A comparison of the SAXS-based curves shows a broader transition for the glass with the higher hydroxyl concentration, which is reflected by the fitting parameters of the model. The fit parameters are sensitive to the width and the details of the shapes of the curves.

4. Conclusion

We have presented three different applications of small-angle X-ray scattering measurements to investigate the density fluctuations that are present at the nanometre scale in silica glass. We have shown that density fluctuations strongly depend on the thermal history on the sample. They are also different for samples with different hydroxyl contents. We also determined the compressibility for four silica samples, corresponding to three different OH contents and two different thermal histories for one of the compositions. Determinations were carried out in the liquid as well as in the glass states, showing a good agreement between different determinations, compatible with a decrease of the isothermal compressibility with increasing temperature and also with increasing OH content. Finally, we took advantage of the sensitivity of SAXS measurements to characterize structural relaxation in the glass transition region and we performed temperature scanning SAXS measurements as an alternative to temperature scanning calorimetry measurements. A detailed analysis provided information about the position, width and shape of the glass transition.

We thank O. Geyamond, S. Arnaud and B. Caillot (Laboratoire de Cristallographie, Grenoble) for technical assistance, and J.-F. Bérar (Laboratoire de Cristallographie, Grenoble) for assistance in using beamline BM02. We also thank the ESRF staff for operating the synchrotron radiation facilities and Marc Vallée (Physics Department, Mount Allison University) for critical reading of the manuscript.

References

Agarwal, A. & Tomozawa, M. (1995). *J. Am. Ceram. Soc.* **78**, 827–829.
Brückner, R. (1970). *J. Non-Cryst. Solids*, **5**, 123–175.
Brüning, R. (2003). *J. Non-Cryst. Solids*, **330**, 13–22.
Brüning, R., Levelut, C., Faivre, A., Le Parc, R., Simon, J.-P., Bley, F. & Hazemann, J.-L. (2005). *Europhys. Lett.* **70**, 211–217.
Champagnon, B., Chemarin, C., Duval, E. & Le Parc, R. (2000). *J. Non-Cryst. Solids*, **274**, 81–86.
Curro, J. J. & Roe, R.-J. (1984). *Polymer*, **25**, 1424–1430.
Diu, B., Guthmann, C., Lederer, D. & Roulet, B. (1989). *Elements de Physique Statistique, Collection Enseignement des Sciences*, 37. Paris: Hermann.
Geissberger, A. E. & Galeener, F. L. (1983). *Phys. Rev. B*, **28**, 3266–3271.
Hodge, I. M. (1994). *J. Non-Cryst. Solids*, **169**, 211–266.
Laberge, N. L., Vasilescu, V. V., Montrose, C. J. & Macedo, P. B. (1973). *J. Am. Ceram. Soc.* **56**, 506–509.
Le Parc, R., Champagnon, B., David, L., Faivre, A., Levelut, C., Guenot, Ph., Hazemann, J.-L., Rochas, C. & Simon, J.-P. (2002). *Philos. Mag. B*, **82**, 431–438.
Le Parc, R., Champagnon, B., Guenot, Ph. & Dubois, S. (2001). *J. Non-Cryst. Solids*, **293–295**, 366–369.
Le Parc, R., Levelut, C., Pelous, J., Martinez, V. & Champagnon, B. (2006). *J. Phys. Condens. Matter*, **188**, 7507–7527.
Levelut, A. M. & Guinier, A. (1967). *Bull. Soc. Fr. Minéral. Cristallogr.* **90**, 445–451.
Levelut, C., Faivre, A., Le Parc, R., Champagnon, B., Hazemann, J.-L., David, L., Rochas, C. & Simon, J.-P. (2002). *J. Non-Cryst. Solids*, **307–310**, 426–435.
Levelut, C., Faivre, A., Le Parc, R., Champagnon, B., Hazemann, J.-L. & Simon, J.-P. (2005). *Phys. Rev. B*, **72**, 224201.
Polian, A., Vo-Thang, D. & Richet, P. (2002). *Europhys. Lett.* **57**, 375–381.
Renninger, A. L. & Uhlmann, D. R. (1974). *J. Non-Cryst. Solids*, **16**, 325–327.
Roe, R.-J. & Curro, J. J. (1983). *Macromolecules*, **16**, 428–434.
Soldo, Y., Hazemann, J.-L., Aberdam, D., Inui, M., Tamura, K., Raoux, D., Pernot, E., Jal, J.-F. & Dupuy-Philon, J. (1998). *Phys. Rev. B*, **57**, 258–268.
Tool, A. Q. & Eichlin, C. G. (1931). *J. Am. Ceram. Soc.* **14**, 276–308.
Weinberg, D. L. (1963). *Phys. Lett.* **7**, 324–325.
Wendorff, J. H. & Fischer, E. W. (1973). *Kolloid-Z. Z. Polym.* **251**, 876–883.
Wright, A. C., Hulme, R. A. & Sinclair, R. N. (2005). *Phys. Chem. Glasses*, **46**, 59–66.